2014•2015

FACULTEIT GENEESKUNDE EN LEVENSWETENSCHAPPEN

master in de biomedische wetenschappen

Masterproef

Defining the synergetic pattern of composites for sensing volatile organic compounds

Promotor :
Prof. dr. Patrick WAGNER

Promotor :
Prof.dr. PETER LIEBERZEIT

Wim Cuypers

Scriptie ingediend tot het behalen van de graad van master in de biomedische wetenschappen

2014•2015
FACULTEIT GENEESKUNDE EN LEVENSWETENSCHAPPEN
master in de biomedische wetenschappen

Masterproef

Defining the synergetic pattern of composites for sensing volatile organic compounds

Promotor :
Prof. dr. Patrick WAGNER

Promotor :
Prof.dr. PETER LIEBERZEIT

Wim Cuypers

Scriptie ingediend tot het behalen van de graad van master in de biomedische wetenschappen

universiteit hasselt | Maastricht University

Table of Contents

Preface

First, I would like to thank Prof. Dr. Peter A. Lieberzeit for his support and guidance during the whole course of my Master thesis. I have learnt a lot of him, both practical skills and theoretical knowledge. His passion in pursuing science, and his attitude toward career and life inspired me to experience science in a different way.
I would also like to pay tribute to Prof. Dr. Patrick Wagner for providing me the extraordinary chance to expand myself in this interesting setting accompanied with a great atmosphere.
My gratefulness also goes to the Department of Analytical Chemistry – Chemical Sensors and Rapid Analysis, for giving me the great opportunity of finalizing my master program in the beautiful city of Vienna.
I am also grateful towards the Erasmus+ program, which made it financially and practically feasible to pass through this experience.
I would also like to pay tribute to my coworkers in the lab. They were always very friendly and willing to help me when they could. My special appreciation is dedicated to Yannick Eurlings and Cédric Libert. Without their help, finalizing my thesis would not have been possible. They were also responsible for the fact that working on my thesis was a pleasure.
I am very grateful towards Dr. Stephan Puchegger who helped me to analyze the Scanning Electron Microscopy samples. Last but not least. I want to thank my soccer team ASK Ober Sankt Veit and my church community ICF Wien, which both introduced me into the Viennese culture and made me feel very welcome.

Abstract

Introduction: Volatile organic compounds (VOCs) are often considered an incalculable cause for disorders such as sick building syndrome (SBS). For this reason, there is a high need for a sensor enabling the detection of these chemicals at relevant concentrations. Preliminary experiments demonstrated the feasibility of detecting VOCs through recognition by a combination of polyurethane (PU) molecularly imprinted polymers (MIPs) and silver sulfide (Ag_2S) nanoparticles. A novel synthesis method for Ag_2S NPs is presented here and the response pattern of both MIPs and composites will be evaluated using quartz crystal microbalance (QCM) for relevant concentrations of 1-butanol.

Materials and Methods: Dropwise addition of silver nitrate ($AgNO_3$, 8mM) to sodium thiosulfate ($Na_2S_2O_3$, 20mM) results in the formation of Ag_2S NPs. Morphology and composition of these nanostructures are analyzed by means of scanning electron microscopy (SEM). NPs are then isolated and incorporated in a PU-MIP network that sensitively binds 1-butanol. The molar ratio of PU to NP equals 1. After deposition onto dual electrode quartz discs, QCM is used to evaluate the binding pattern of 1-butanol. An identical evaluation is made for MIPs alone.

Results: SEM results indicate the formation of Ag_2S NPs. Moreover, composites have shown to bind more sensitively to 1-butanol than MIPs. Increasing concentrations of 1-butanol yield larger responses after standardization to the same layer height. Repeated experiments have shown no significantly different QCM results, highlighting the reproducibility of this set-up.

Conclusions and Discussion: Ag_2S NPs can be synthesized by an alternative method avoiding drawbacks associated with other techniques (i.e. H_2S method). It bypasses the workplace safety issues related to H_2S and moreover, it allows for a more controlled chemical reaction. MIP composites with such nanoparticles yield higher gravimetric responses compared to the MIPs alone.

Samenvatting

Introductie: Vluchtige organische stoffen (VOS) worden vaak aanzien als een onberekendbare oorzaak voor stoornissen zoals het „sick-building syndroom". Daardoor is er een hoge nood voor een sensor die deze chemicaliën op relevante concentraties kan meten. Voorafgaande studies bewezen de mogelijkheid voor het detecteren van VOS door herkenning met behulp van een combinatie van polyurethaan (PU) molecular imprinted polymers (MIPs) en zilver sulfide nanopartikels (Ag_2S NPs). Een nieuwe synthese methode voor Ag_2S NPs wordt hier gepresenteerd en het responspatroon van zowel MIPs als composieten zal geëvalueerd worden met behulp van de kwarts-microbalans (QCM) techniek voor relevante concentraties van 1-butanol (1-BuOH).

Materialen en Methoden: Druppelsgewijze toediening van zilver nitraat ($AgNO_3$, 8mM) aan natrium thiosulfaat ($Na_2S_2O_3$, 20mM) resulteert in de vorming van Ag_2S NPs. Morfologie en compositie van deze nanostructuren worden geanalyzeerd met behulp van Rasterelectronenmicroscopie (SEM). NPs worden dan geïsoleerd en geïncorporeerd in een PU-MIP netwerk hetgeen 1-butanol selectief bindt. De molaire verhouding van PU ten opzichte van NPs bedraagt 1. Na depositie van het composiet op tweeledig-elektrode bezittende kwarts schijfjes wordt de QCM techniek gebruikt om het bindingspatroon van 1-BuOH vast te stellen. Een gelijkaardige evaluatie is ook gemaakt voor MIPs alleen.

Resultaten: SEM resultaten tonen de vorming van Ag_2S NPs aan. Bovendien vertonen composieten een grotere gevoeligheid voor 1-butanol in vergelijking met MIPs. Toenemende concentraties 1-BuOH leiden tot grotere signalen na standaardisatie voor dezelfde laagdikte. Herhaaldelijke experimenten toonden geen significante verschillen in QCM resultaten, hetgeen de reproduceerbaarheid van deze set-up aantoont.

Conclusie & Discussie: Ag_2S NPs kunnen gesynthetizeerd worden door een alternatieve methode die de nadelen die gepaard gaan met andere technieken (bv. H_2S methode) vermijdt. Het omzeilt de veiligheidsproblemen die gepaard gaan met H_2S gebruik. Tevens is het gemakkelijker om de chemische reactie te controlleren. MIP composieten met zulke nanopartikels leveren hogere gravimetrische responsen in vergelijking met MIPs alleen.

1. Introduction

Over the last decades, large numbers of building inhabitants have been suffering from poor air quality. The situation where acute health and comfort effects are related to the time spent in the building is defined as the "sick building syndrome (SBS)" (1-3). Remarkable for this disorder is the absence of an explicit illness or cause. Nonetheless, many clinically definite symptoms are associated with SBS. Among them, neurotoxic effects, mucous membrane irritation and asthma (-related symptoms) are the most frequent signs (1, 4). Volatile organic compounds (VOCs) can be seen as an incalculable source responsible for the development of these problems (5). Therewith, various other chemical contaminants, biological contaminants, insufficient ventilation, psychological factors and electromagnetic radiation are considered potential risk factors (6-8). In this work, the focus will be on the role of VOCs and the detection. More specifically, the profile of 1-butanol will be assessed. The choice for this VOC is quite straightforward since it is a rather simple and ubiquitous molecule which makes it more facile to detect. In addition, this compound is known to be involved in abiotic processes. According to the Occupational Safety and Health Administration (OSHA), the permissible exposure limit (PEL) is 100 parts per million parts of air (ppm) as an 8-hour time-weighted average (TWA). Starting from 1-BuOH, it is possible to expand procedures towards more complicated and less ordinary VOCs.

VOCs are chemicals originating from both biological and anthropogenic sources (9). A common feature all VOCs share is the presence of carbon in their backbone. Moreover, these organic compounds contain other elements such as hydrogen, oxygen, nitrogen and sulfur to name but a few (10). Furthermore, they are characterized by a low boiling point at standard atmospheric pressure. Consequently, high vapor pressure at normal temperature explains their readily evaporation. Liberation of VOCs in air occurs by evaporation from various products at room temperature (11). A list of relevant VOCs and their origin is displayed in Table 1.1 (12). These organic compounds are classified as air pollutants. Unquestionably, particular VOCs interact with nitrogen oxides (NO) arising mostly from combustion of fossil fuels. The end product of this reaction is nitrogen dioxide (NO_2). In presence of sunlight, NO_2 is broken down by a process called photolysis. This results into the formation of ground-level ozone (O_3), the main component of smog. Upper-atmosphere O_3 contributes to the fencing of the earth from detrimental rays originating from the sun (13). On the other hand, ground-level O_3 is harmful to human health. Simultaneously, reaction between VOCs and NO_2 results in the synthesis of toxic and irritating compounds such as peroxyacetyl nitrate (PAN). In the atmosphere, these pollutants decompose into NO_2 and peroxyethanoyl radicals.

PANs exhibit a lachrymatory function, meaning they are capable of causing secretion of tears (14). Besides, they are featured by their mutagenic behavior ultimately giving rise to skin cancer (15)

Table 1.1. Environmentally important VOCs and their appearance.

VOC	Origin
Biological	
Methane	Microorganisms
Terpenes	Plants
Benzene	Volcanoes, forest fires
Anthropogenic	
Acetone	Paints, varnishes, nail polish remover
Benzene	Tobacco smoke, stored fuels, exhaust from cars
Chlorofluorocarbon	Cleaning products, refrigerants
Ethylene acetate	Paintings
Formaldehyde	Adhesives, paints, wall boards, ceiling boards
Glycol ether	Paintings
Hexane	Gasoline
Methylene chloride	Adhesive removers, aerosol spray paints
Perchloroethylene	Dry cleaning
Styrene	Insulation, plastics, rubber
Tetrachloroethene	Dry cleaning, industry
Toluene	Paint thinners
Trichloroethane	Solvents

Exposure to an excess of VOCs, both short- and long-term, induces a wide range of health problems. Emesis and conjunctive irritation are just a few key examples of early symptoms associated with it. Other examples include headaches, fatigue and dizziness (16). Besides, it has also been proven that residential exposure to VOCs enhances the risk of developing asthma/atopic disease (1, 17). In a later stage, various vital organs such as liver and kidney can be affected (18). There also is an increased risk for central nervous system (CNS) damage.

At long last, these detrimental organic compounds augment the chance to develop cancer and eventually for causing death (6, 12, 18). Alongside of prejudicial health effects, VOCs are also involved in some disadvantageous environmental processes. They impair multiple ecosystems as well as sensitive vegetation (14). Because of its great interest for human society, detection and monitoring of VOCs is essential nowadays. This can be achieved with the aid of a sensor, a device deriving its name from the Latin word *sentire*, literally meaning "to feel". Figure 1.1 gives an impression of the general structure of a sensor.

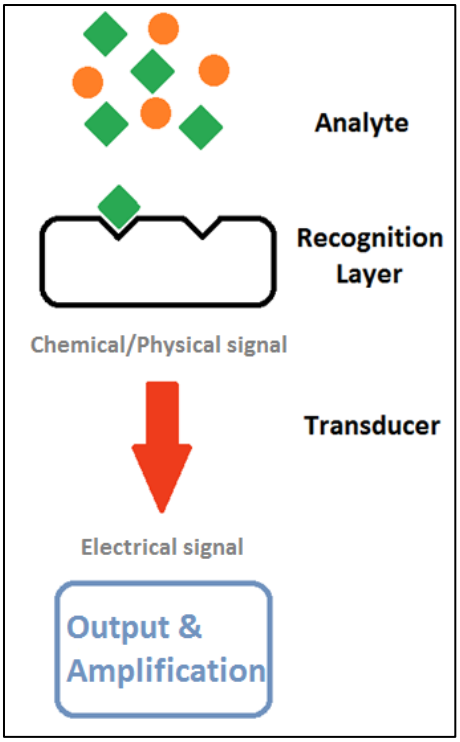

Figure 1.1. General scheme of a sensor.

One distinguishes three important (sub-) classes of sensors, namely biosensors, physical sensors and chemical sensors. Here, the latter will be highlighted inasmuch the goal is to derive information about the chemical environment using a chemical recognition element. Chemical sensors are capable to convert alterations in chemical surroundings to an unambiguous readout signal, mostly electrical or optical. First of all, it consists of a recognition element, capable of detecting the desired chemical compound. In contrast to biosensors, the recognition element will not be of biological origin. Instead, it has its roots in the chemical world.

With the rise of biomimetic materials such as aptamers and molecularly imprinted polymers (MIPs) as recognition elements, the boundary between a biosensor and chemical sensor is rather vague. Since the sensor presented here exhibits a recognition layer composed of both nanoparticles and MIPs, it can be considered as a biomimetic chemical sensor. Such a coating consisting of these two components is denoted as "composite". Its build-up consists of two constituents expressing distinct chemical and/or physical properties which, when unified, generates a material having new properties different from the separate parts. Binding events will evoke a response by the recognition layer which is subsequently converted by a transducer. After this translational process, one is able to interpret and, if desired, further process acquired data. The final result is an electrical signal which gives quantitative indication of the presence of analyte in the sample. Applied to our example, it gives information about the concentration of VOCs near to the detection platform (19).

Unfortunately, detection and quantitative determination of these VOCs is difficult because they are present in very low concentrations, usually in the ppb range. Mass spectrometry (MS) and Fourier transform infrared (FTIR) spectrometry are two notable techniques used for monitoring VOCs (20). However, they have some drawbacks such as their high cost and time demands. Furthermore, they are usually only suitable for offline analysis.

Quartz crystal microbalance (QCM) can be seen as a solution to overcome these problems. This technique makes use of the fundamental frequency (alternatively called "eigenfrequency") of quartz crystals, meaning that application of alternating voltage results in oscillations at a certain characteristic frequency. When a binding event takes place, extra mass is appended to the surface. The result is a decrease in frequency. QCM offers a quick response accompanied with high sensitivity. Besides, online monitoring of analytes can be achieved by this label-free real-time method (20, 21).

The goal is to develop a sensor consisting of polyurethane molecularly imprinted polymers (PU MIPs) and silver sulfide nanoparticles (Ag_2S NPs) in order to achieve optimal detection of volatile organic compounds using QCM. A schematic representation of such a sensor is given in Figure 1.2. This work will mainly concentrate on the detection of 1-butanol but the procedures can be extended to a wide range of VOCs.

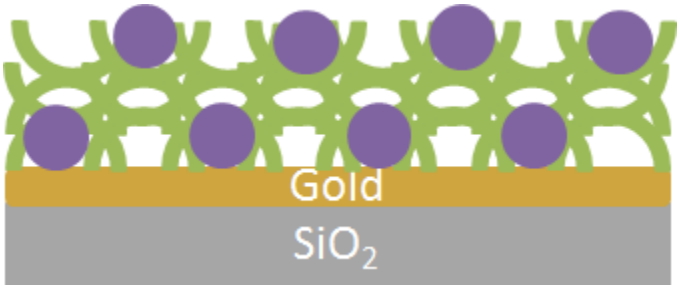

Figure 1.2. Schematic representation of a NP-MIP composite.

MIPs have gained considerable interest over the last decades (22). This is brought about by their potential to obtain very stable synthetic receptors for a variety of target molecules. They mimic molecular recognition of natural receptors (23). Both types of receptors, biological and synthetic, can be used repetitively benefiting from reversible non-covalent interactions with its target (24).

Molecular recognition can be regarded as lock and key binding postulated by Emil Fischer in 1894 (25). This process is displayed in Figure 1.3. He stated that only substrates having the precise structure fit active sites (holes) of an enzyme. Actual binding can be considered the result of a plethora of weak bonds such as hydrogen bridges, π–π interactions and ionic forces. These bonds lead to very strong interactions between biomolecules outlining the importance of biological receptors (24). If they exhibit so many advantageous properties, why preferring MIPs over biological receptors? First of all, the biological receptors are comparably instable to variable chemical environments limiting their efficacy solely to certain – physiological – temperatures and pH values. Besides, not all target molecules are able to bind biological molecules with sufficient selectivity and affinity. Frequently, they require tiresome synthesis steps (26). Moreover, the price of biological receptors can be very high, among others because of the need for laboratory animals (27). MIPs, on the other hand, exhibit high affinity, selectivity, stability and versatility (28) at comparably low cost (29). During their synthesis, functional monomers arrange around a template molecule. Self-assembly leads to the formation of a pre-polymerization complex. In the next step, cross-linkers and a radical initiator are added to the mixture. They provide a hard polymeric material after polymerization. After the template molecule is washed away, the resulting cavities permit successive binding of the target molecule (30). In this work, polyurethane (PU) will be employed for the synthesis of MIPs.

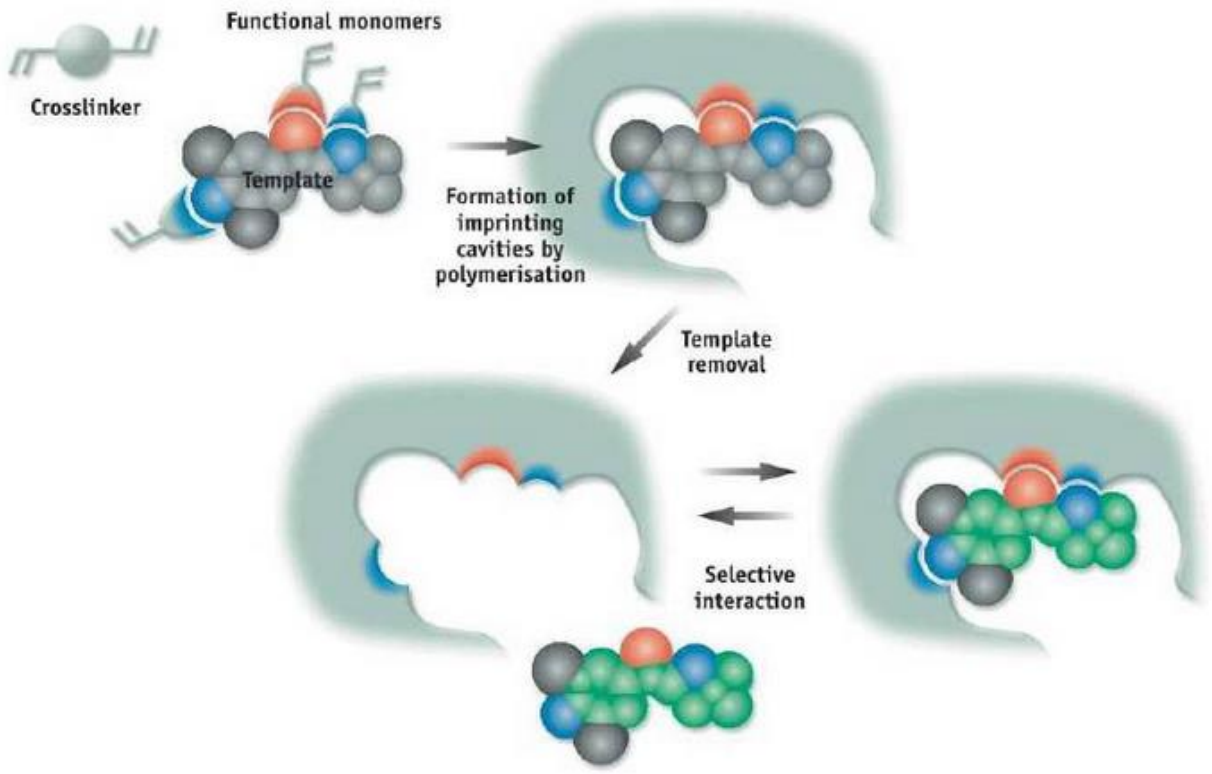

Figure 1.3. The basic principles of molecular imprinting. (Source: Biotage AB, Sweden)

MIPs have proven useful for detecting various analytes (nicotine, histamine, somatostatin) in aqueous environment (31, 32). However, MIPs alone are insufficiently sensitive for sensing VOCs at relevant low concentrations. Hence, NPs are incorporated in the recognition elements of the chemical sensors. These particles are characterized by a size ranging from 1 to 100 nm. Due to their large surface-to-volume ratio, NPs exhibit interesting properties. Composites evoke increased sensitivity due to high contact surface area. Furthermore, they lead towards increased selectivity owing to affinity modifications.

Preliminary experiments already demonstrated sensitivity of soft metal sulfide nanoparticles towards soft thiol compounds (e.g. butane thiol). The term "soft" indicates a large, easily polarizable particle with low charge density. Here, however, detection of an alcohol (1-butanol) is required. Trials benefiting molybdenum disulfide (MoS_2), copper sulfide (Cu_2S) and silver sulfide (Ag_2S) surfaces demonstrate the highest selectivity towards 1-butanol in case of Ag_2S NPs. (33, 34). Interaction between metal sulfide nanoparticles and alcohols is established by polar-polar interactions between sulfur and hydroxyl groups.

Silver sulfide appears in two different forms in nature. Monoclinic acanthite is known to be the stable form of silver sulfide below 173°C while cubic argentite represents the steady counterpart at temperatures above this value. Preliminary experiments demonstrate the synthesis of MIP-NP composites, which can be used for sensing VOCs. More precisely, silver sulfide (Ag_2S) NPs are prepared using H_2S precipitation method (33). After dissolving silver nitrate ($AgNO_3$) in anhydrous ethanol, the mixture was purged with H_2S gas. Hereby, the solution undergoes a color shift. The slightly yellow/orange color is attributed to Ag_2S NP synthesis. These composites are employed for sensing 1-butanol, a simple VOC.

Inspired on the synthesis of Ag_2S layers formed on polypropylene by Krylova in 2013 (35), a novel method for the synthesis of silver sulfide (Ag_2S) nanoparticles in solution will be presented here. This way, it is possible to avoid the adverse effects of working with H_2S. An example of these pullbacks is the toxicity accompanied with this technique, being in the range of hydrogen cyanide (HCN) and carbon monoxide (CO). The toxic effect is attributed to the ability of H_2S to form a complex bond with iron in the mitochondrial cytochrome enzymes. As a result, cellular respiration is inhibited.

In the future, investigation of responses towards molecules with same chain length, but different functionality have to be done, e.g. with butane thiol. Moreover, experiments exploring selectivity introduced by MIPs are necessary. This can e.g. be done by QCM measurements comparing 1-butanol with 2-butanol. At last, MIP/NP composites of more defined morphology can be generated. Their gas sensing properties will be assessed by either immobilizing NP on sensor substrates and depositing MIP layers onto them with systematically variable height, or by developing strategies to synthesize core-shell nanoparticles with affinity cores and different MIP shell thicknesses.

2. Experimental

2.1. Materials

Quartz crystals were obtained from Great Microtama Electronics, Indonesia and have a fundamental frequency of 10 MHz. Furthermore, they are characterized by a cutting angle of 35°15'±3 (AT cut) and a diameter of 14 mm. Onto these substrates electrode structures are deposited by screen printing brilliant gold paste purchased from Heraeus containing 12% gold. After deposition, crystals are baked in an oven at 400°C for four hours. Quartz crystals before and after printing are depicted in Figure 2.1. Both sides of crystals are coated with circular electrodes. One electrode pair serves as a reference while the other functions as working electrode for the actual measurement.

Figure 2.1. Pictures of blank quartz crystal (left) and gold-printed quartz crystal (right).

Silver nitrate ($AgNO_3$) and sodium thiosulfate ($Na_2S_2O_3$) were purchased from Applichem Panreac (IWT Companies). 4,4'-methylenediphenyl diisocyanate (MDI, alternatively denoted to as diphenylmethane 4,4'-diisocyanate (DPDI)), phloroglucinol (POL), 1,4-diazabicyclo[2.2.2]octane (DABCO), toluene, hydrogen peroxide (H_2O_2), ethanol, sulfuric acid (H_2SO_4), tetrahydrofuran (THF) and sodium hydroxide (NaOH) were used as received from Merck KGaA. 4,4'-Isopropylidenediphenol (Bisphenol A, BPA, ≥95%) and (3-Aminopropyl) triethoxysilane (APTES, ≥98%) were purchased from Sigma-Aldrich. 1-butanol was obtained from VWR. Polyvinylpyrrolidone (MW: 58,000 Da) was purchased from Alfa Aesar GmbH&Co KG. All untreated solvents used for synthesis were of HPLC/Analytical grade and were used as received. APTES was stored under argon gas pressure prior to use. Milli-Q grade water was used unless otherwise specified.

2.2. Techniques

2.1.1. Scanning Electron Microscopy (SEM)

Silver sulfide nanoparticles are synthesized in an aqueous solution followed by deposition to a measuring platform. This way, they are not covalently attached to the surface. As a result, characterizing them using Atomic Force Microscopy (AFM) (by contact mode or tapping mode) would result in displacement by the cantilever tip ultimately giving rise to blurry pictures. Scanning electron microscopy is reckoned to be a powerful tool for circumnavigating this. A schematic representation is given in Figure 2.2.

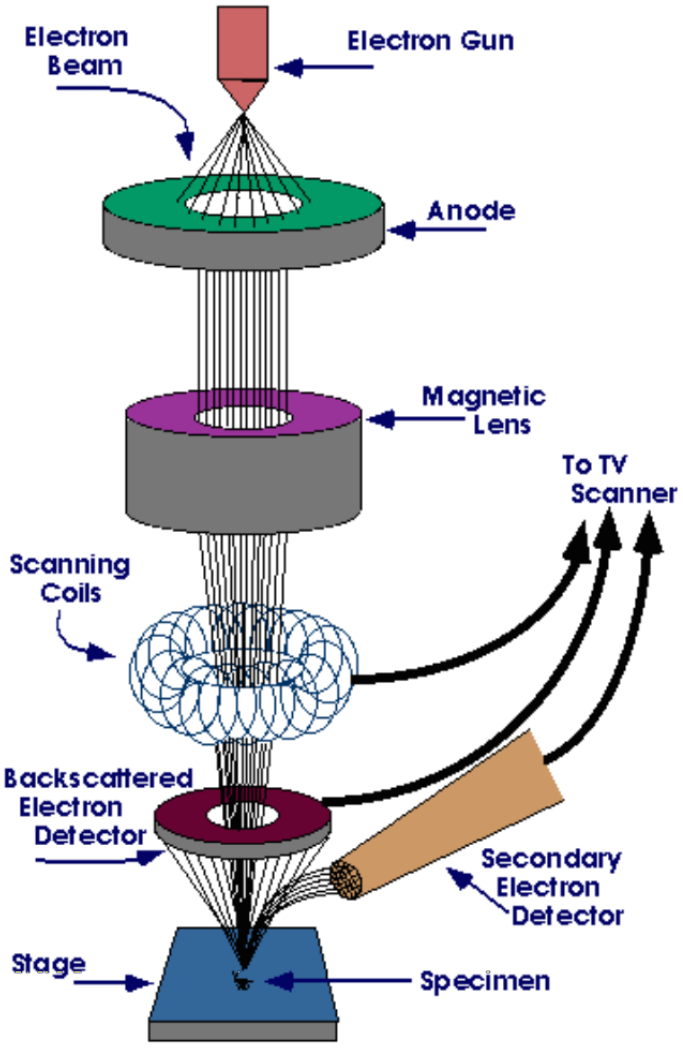

Figure 2.2. Schematic representation of SEM technique. (Source: Purdue University; Radiological and Environmental Management)

Ordinary light microscopes have an optimal magnification up to 1000X. Furthermore, their resolution is limited to a minimum of ~200 nanometers, which is too low for accurate detection of nanoparticles being smaller than this value. The use of electrons rather than visible light gets around this problem, because they are characterized by lower wavelengths. This allows one to obtain resolutions of sub-nanometer level. On top of that, it is possible to achieve depth of field with a factor 1000 more compared to conventional light microscopes.

SEM relies on an electron gun focusing electrons through a vacuum tube onto the sample surface. They either pass the sample or interact with the atoms. The former ones are not meaningful for creating the image. When electrons collide with the surface, this leads to two types of interactions with the sample, namely elastic and inelastic collisions. Elastic collisions can be described with a "billiard-ball" model, since the electrons bounce back from the sample without noteworthy loss of kinetic energy. This happens when minuscule electrons will be rejected after collision with the nuclei of larger atoms leading to so-called "primary backscattered electrons (BSE)". The probability of evoking an elastic collision is more likely for elements having higher atomic (Z) number generally characterized by a larger scattering cross-section. However, not all electrons will collide with atoms without deprivation of energy. These electrons have said to be subjected to inelastic scattering. In some cases, electrons may lose some energy after collisions with atom nuclei. More likely is the event where incident electrons interact with the electron clouds of atoms in the sample. As a result, electrons having significantly lower kinetic energy than the citation electrons will be emitted constituting so-called secondary electrons. This type of electrons allows one to determine the topography and morphology of the sample. Through the formation of secondary electrons, atoms in the sample will become ionized. Removal of an inner-shell electron by the electron beam leads to the formation of a hole. An electron of an outer shell will relaxate to occupy this vacancy resulting in the release of X-rays. This type of radiation provides information about the composition and amount of certain elements in the sample. Utilizing SEM, it is possible to determine three-dimensional structures where AFM solely gives rise to the acquirement of two-dimensional images. As the electrons cause charging of the surface, SEM requires the presence of a conducting surface. If this is not the case by itself, it is possible to cover the surface with a thin conducting film. It should also be noted that the samples have to be solid and dry since SEM benefits charged electrons flowing through a vacuum.

2.1.2. Quartz Crystal Microbalance

General principles

In 1880, Jacques and Pierre Curie were the first to describe the effect where application of mechanical stress to some crystals (i.e. quartz, ceramics) leads to the generation of an electrical voltage proportional to this pressure. This property is called the piezoelectric effect. More specifically, when subjecting a material to mechanical stress results in a voltage, it is called the direct effect. Likewise, applying an electric field to such a crystal gives rise to a mechanical deformation and is denoted as the inverse piezoelectric effect. Piezoelectric crystals have their asymmetric build-up in common. Furthermore, they are characterized by an insulating behavior.

Quartz (SiO_2) crystals are the most prominent candidates for the crystal microbalance technique. First of all, the material is found in abundance in nature. Besides, it is non-toxic and can be used for very accurate measurements making it possible to detect minor mass changes on its surface. The structure of quartz and its related piezoelectric effect is given in Figure 2.4.

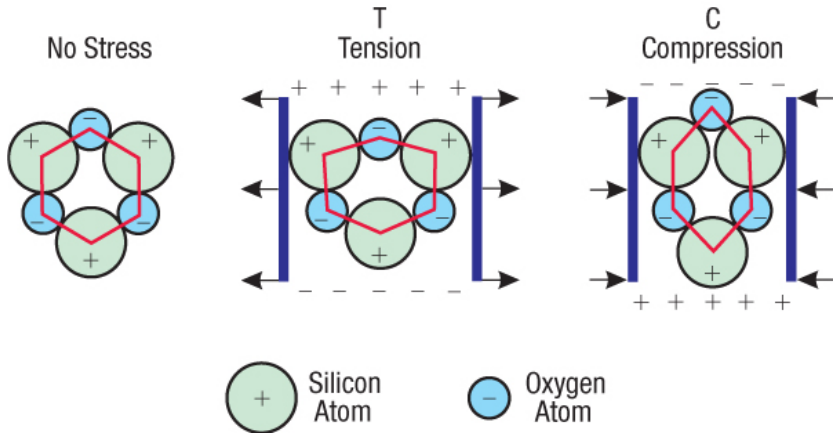

Figure 2.4. Piezoelectric effect on a quartz crystal. (Source: Center for Scientific Creation)

As visualized in the picture above, quartz is composed of silicon and oxygen atoms. In equilibrium, positive and negative charges cancel out each other. After subjecting a quartz crystal to pressure, atoms are displaced. This automatically leads to a shifting of charges ultimately heading to accumulation on contrary faces.

The result is an electrical polarization (P) which is proportional to the dipole moment ($Q.h$) between the two borders of the crystal. Q is denoted as the full charge on one side while h is the height of the layer. There also exists a reciprocal relationship between the amount of polarization and the volume (V) of the quartz crystal slice.

$$P = \frac{\mathrm{Q.h}}{\mathrm{V}}$$

It has been said that application of a direct voltage results in a distribution of charges in a quartz crystal. Without changing the voltage, charges will remain in a fixed position. However, when an alternating voltage is applied, charges can redistribute dependent on the voltage extent. The result is an oscillation of the quartz crystal since the specimen will make repeatedly vibrations. Binding of mass onto the QCM leads to an alteration of the fundamental frequency. In the middle of the twentieth century, Sauerbrey indicated the relation between the resonance frequency and the alteration in surface load. Its equation can be written as:

$$\Delta f = \frac{-2 f_0^2}{A \, r_{crystal} \, v_{crystal}} \cdot \Delta m = -\frac{\Delta m}{m_0} \cdot f_0$$

Δf: change in resonance frequency
f_0: fundamental frequency
Δm: change in mass
m_0: mass of uncoated quartz
A: surface area
$\rho_{crystal}$: quartz density
$v_{crystal}$: speed of sound in quartz

Because of this breakthrough, quartz resonators have found their way into the world of detection platforms. Their function can be described as thin-layered microbalances with high sensitivity for detecting various analytes. In order to determine whether or not chemicals bind to the detection platform, quartz crystal microbalance (QCM) can be seen as a protrusive characterization method. Its simplicity, cost effectiveness and real time behavior are only some of the many advantages of this measuring procedure. After application of an alternating voltage between the electrodes, blank (uncoated) QCMs undergo mechanical oscillations at their proper eigenfrequencies. At this frequency, the system oscillates in absence of any damping or driving force. Functionalization of these samples will result in additional mass and thus in a decrease in natural frequency. After a significant frequency drop, one can state that a binding event has taken place. The extent of the frequency drop dependents on mass size, following the Sauerbrey equation, denoted earlier. This observation allows one to monitor binding events taking place, but only for films that are rigid, homogeneous and sufficiently thin ($\Delta f/f_0 < 0.05$). A representation of a bare crystal and a coated one are reproduced in Figure 2.5.

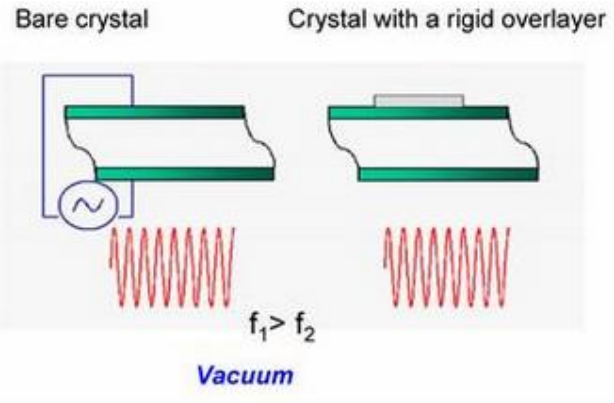

Figure 2.5. Schematic representation of blank and coated QCM crystals and their related frequencies. (Source: Swiss Federal Institute of Technology Zürich)

In numerous cases, however, the absorbed films cannot be considered rigid or homogeneous, causing other parameters to be of relevance as well; the film's viscoelastic properties, thickness and density should then also be taken into consideration. Viscoelastic films tend to dampen the sensor's oscillation, a phenomenon referred to as *dissipation*, which can be assessed through QCM-D analysis. Here, however, one deals with fairly rigid layers comprising nanoparticles and polyurethane. Therefore, QCM without dissipation monitoring is employed.

Experimental set-up of QCM technique

Exploitation of QCM crystals takes place using a tailor-made oscillator circuit. Frequency measurements are carried out with a 2-channel frequency counter (Agilent Technologies 53131A, 225 MHz) and a laboratory power supply (EA-PS 2032-025). Data acquisition is performed using Read_UniCount, a program routine relying on Labview software. A gas mixing apparatus (Westphal Mess-und Regeltechnik (WMR) 4008) incorporated with mass flow controllers (Brooks Instrument) ensures a gas flow containing the exact amounts of 1-butanol. A schematic representation of the set-up is given in Figure 2.6.

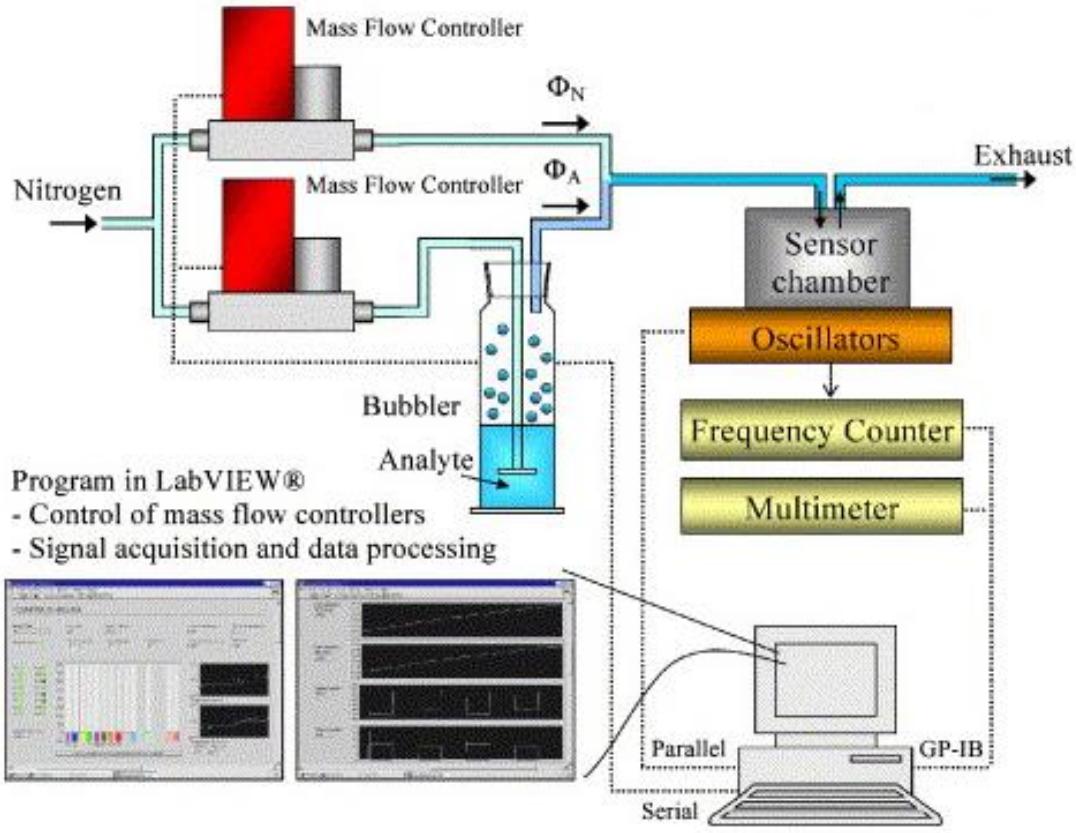

Figure 2.6. Schematic representation of the gas measurement set-up.

As indicated by Figure 2.6, exposing the QCM sample to different concentrations of 1-butanol vapour in air happens by the mixing of an airstream saturated with 1-butanol and a solvent free airstream. Out of the volumes and damping pressures from the solvent, it is possible to calculate the exact concentration of 1-butanol at the quartz surface. The formula used for this conversion is written below.

$$[ppm] = \frac{V_{LM}(1 + \frac{P_{LM}}{P_0})}{V_{LM}(1 + \frac{P_{LM}}{P_0}) + V_{Luft}} \cdot \frac{p_{LM}}{p_0} \cdot 10^6$$

V_{LM}: volume of solvent
V_{Luft}: volume of air
P_{LM}: damping pressure of solvent (P_{BuOH} = 6.70 hPa)
P_0: partial pressure of air (~10^5 Pa)

2.3. Methods

2.3.1. Silver sulfide nanoparticle synthesis

First, 20 mM $Na_2S_2O_3$ is dissolved in a PVP/dH_20 solution (0.172 mM, 200mg/20mL). This step is followed by the dissolution of 8 mM $AgNO_3$ in the same solvent resulting in two equivoluminal solutions. Dropwise addition of the latter into the sodium thiosulfate mixture takes place under vigorous stirring to obtain the desired nanoparticle complexes.

Ag_2S NPs in solution are centrifuged for 15 min at 3500 rpm. Next, the supernatant is removed. Particles are dried overnight at 70°C. In a later step, 3.7 mg of these dry NPs are dissolved in 750 µl THF to obtain a 300 mM solution of Ag_2S NPs.

Without the use of PVP, NPs will aggregate to a larger extent. This water-soluble polymer acts as a stabilizer for Ag_2S NPs (36). Besides, sodium thiosulfate is used in excess to achieve NPs instead of large clusters. UV-VIS is employed as control technique to determine if to many larger NP clusters are formed. After administration of the $AgNO_3$ solution to the $Na_2S_2O_3$ solution, the solution turns slightly yellow/orange. A black precipitate is formed immediately if larger concentrations are used or when mixtures are simply added together at once. The latter results in many clusters because nanoparticles cannot be stabilized and will aggregate. Note that Ag_2S NPs are insoluble in many solvents such as ammonia and KCN solution. It do is possible to dissolve them in a hot HNO_3 solution.

2.3.2. Preparation of SEM samples

APTES is employed for immobilizing the home-synthesized Ag_2S NPs to a silicon wafer. In a first step, silicon samples are bathed in an APTES solution. These alkoxysilane molecules will bind the surface because of the presence of hydroxyl group onto its top layer. As a result, covalent silicon-oxide-silicon bonds are established by the withdrawal of alkoxy groups from the APTES molecules caused by the hydroxylated surface. Silver sulfide NPs will interact with the amino groups offered by the abundant present APTES molecules resulting in adequate NP coverage of the silicon wafer.

SEM measurements require thoroughly cleaned silicon substrates. A visual overview of the cleaning process applied in this thesis is displayed in Figure 2.7. In a first step, the wafers are immersed in a 6 M sodium hydroxide (NaOH) solution for one minute at room temperature. This is followed by excessive rinsing using distilled water. Next, the samples are placed in a beaker containing hydrogen peroxide (H_2O_2). After placing the glassware in a sonicating bath, sulfuric acid (H_2SO_4) is added to it until the ratio of H_2O_2 to H_2SO_4 amounts 2:3 and the mixture is denoted as "piranha solution". Immediately after the two compounds are combined, samples are placed in the sonicator for fifteen minutes.

Thereafter, the wafers are rinsed with distilled water and blow-dried using argon gas followed by placing them to an Erlenmeyer flask containing 20 mL water-free toluene. The polished surface of the silicon has to face upwards since this side is the one which becomes functionalized.

Subsequently, 500 µl (3-Aminopropyl) triethoxysilane (APTES) is added. Air has to be excluded since it will lead to unwanted side reactions. Humidity can dissolve with toluene, which at its turn can impede reactions between APTES molecules. After 4 hours, wafers are removed from the solution followed by intensive rinsing with distilled water. In the end, samples are blow-dried and finally 10 µl of the NP solution (300 mM) is applied on the substrates.

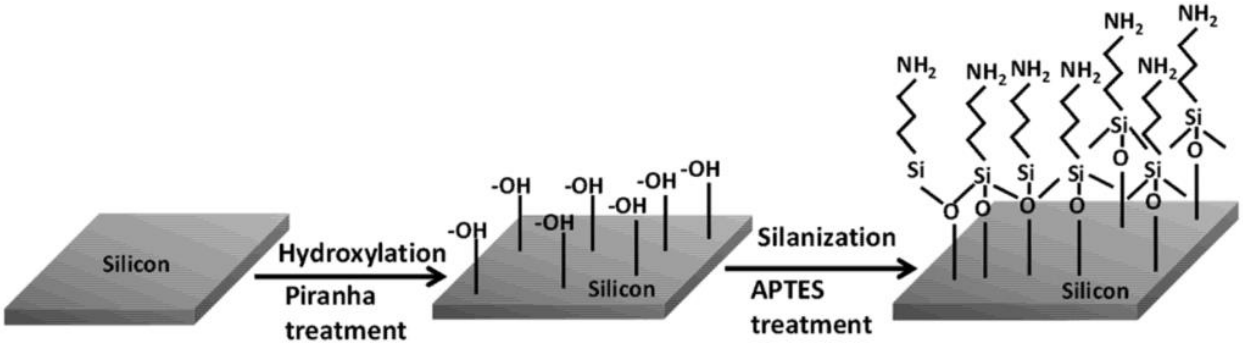

Figure 2.7. Schematic representation of silicon wafer functionalization with APTES molecules after piranha handling. (37)

2.3.4. Polyurethane synthesis

Polyurethane is synthesized according to an already published procedure. 100 mg MDI, 200 mg bisphenol A (BPA), 20 mg phloroglucinol (POL) and 200 µL tetrahydrofuran (THF) are added together in an Eppendorf tube and sonicated for fifteen minutes to obtain a homogeneous mixture. 880 µl THF is then added to 100 µl of this solution. Next, 20 µl of a 0.178 M DABCO solution (in THF) is added to the mixture. To obtain the prepolymerization complex, the batch is heated for ten minutes at 70°C. As indicated by Figure 2.8, hydroxyl groups of BPA and phloroglucinol react with isocyanate groups of MDI monomers. The result is the formation of polymers comprising both molecular units linked by urethane groups. POL allows for crosslinking of the polymers. In order to accelerate the polymerization process and to increase the reproducibility of the experiments, DABCO is added as a catalyst. Self-synthesized PU is used in the production of NIP, MIP and composites.

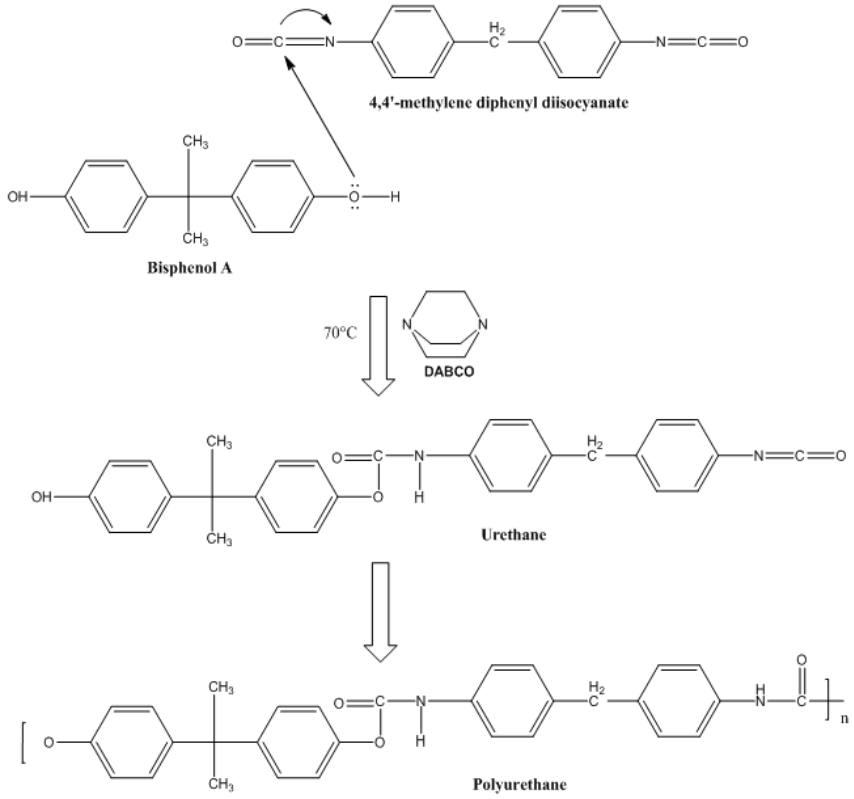

Figure 2.8. Polyurethane synthesis process.

2.3.5. NIP synthesis

Polyurethane, prepared according to the procedure described above, is used for the development of NIPs. 30 µL of the pre-reacted PU solution is dissolved in 970 µL of THF. An extra 30X dilution in THF is performed for this mixture. After spin-coating (5 seconds at 2000 rpm) 5 µL NIP solution onto gold-coated QCM crystals, samples are dried overnight at 70°C.

2.3.6. MIP synthesis

Polyurethane, prepared according to the procedure described above, is used for the development of MIPs. 30 µL of the pre-reacted PU solution is dissolved in 970 µL of 1-butanol. An extra 30X dilution in THF is performed for this mixture. After spin-coating (5 seconds at 2000 rpm) 5 µL MIP solution onto gold-coated QCM crystals, samples are dried overnight at 70°C.

2.3.7. Composite synthesis

500 µl of the 300 mM NP mixture is suspended in 500 µl of the polyurethane-butanol mixture to yield a 1:1 molar ratio. Thereafter, 5 µL of composite solution is spin-coated (5 seconds at 2000 rpm) onto gold-coated QCM crystals. Samples are dried overnight at 70°C. It is however not feasible to coat QCM samples with NPs solely and investigating their response pattern. Because of the fact that Ag_2S NPs are not tending to stick to the gold surface, air and flow results in the displacement of these particles. The outcome is a constantly oscillating signal full of noise. Functionalizing the NPs onto the surface using a coupling agent may provide a solution. However, one has to account for the influence of this cross linker molecule. A simplistic representation of an uncoated, NIP-, MIP-, NP- and composite-coated QCM sample is given in Figure 2.9.

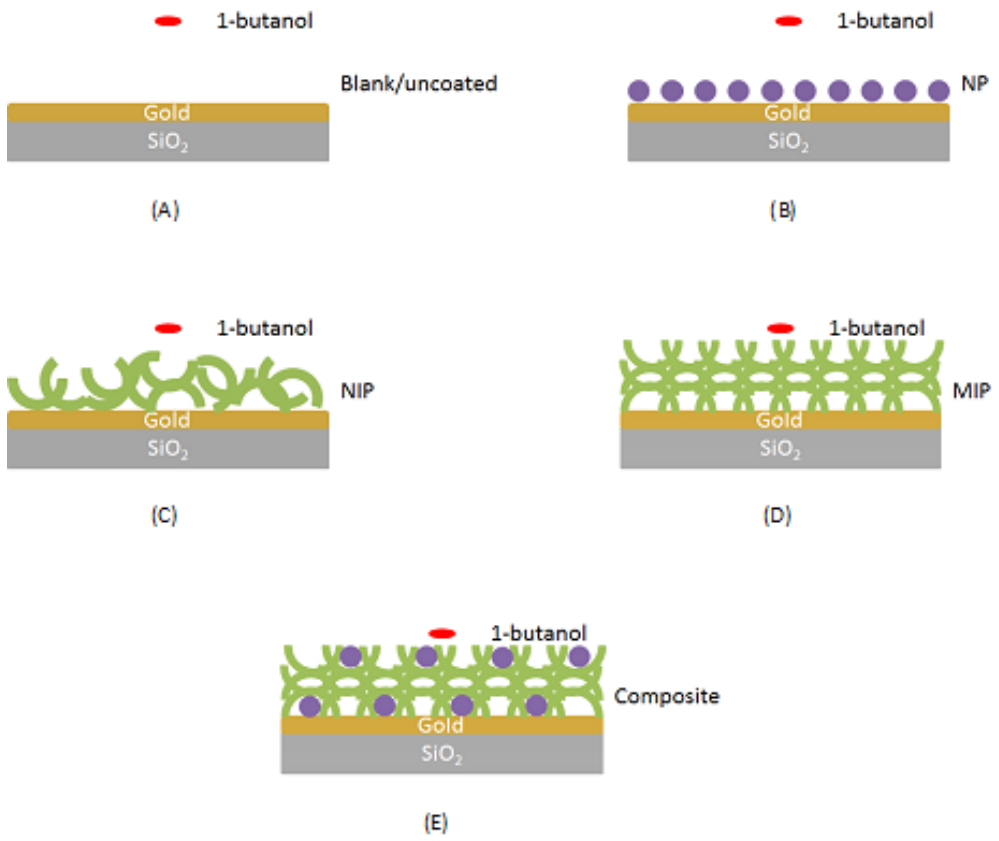

Figure 2.9. General representation of: A) uncoated, B) NP-coated, C) NIP-coated, D) MIP-coated and E) composite-coated QCM samples.

3. Results & Discussion

3.1. Scanning Electron Microscopy

Figure 3.1 demonstrates the presence of nanoparticles on the silicon wafer. Here, one can clearly see clustering of NPs. This effect can be attributed to insufficient stabilizing by PVP. Another explanation can be the too rapidly administration of the silver nitrate solution towards sodium thiosulfate/PVP mixture.

As already explained in the methods section about SEM, secondary electrons allow for establishing the surface topography of the sample surface. The so-called *edge effect* is responsible for this characterization principle. A beam of electrons will penetrate the specimen. Whenever borders of the self-synthesized particles are exposed to such a beam, it is more facile for electrons to leave this place. The outcome is an augmented brightness of the image at this point. In order to declare what kind of particles are formed, primary backscattered electrons (BSE) come into play. Elastic collisions with the Ag_2S particles give rise to signals for silver and sulfide respectively. This is made possible by the fact that the electrons collide with the different elements leading to backscattering out of the sample. It is the atomic number (Z), which is distinctive for the fraction of BSE in the specimen.

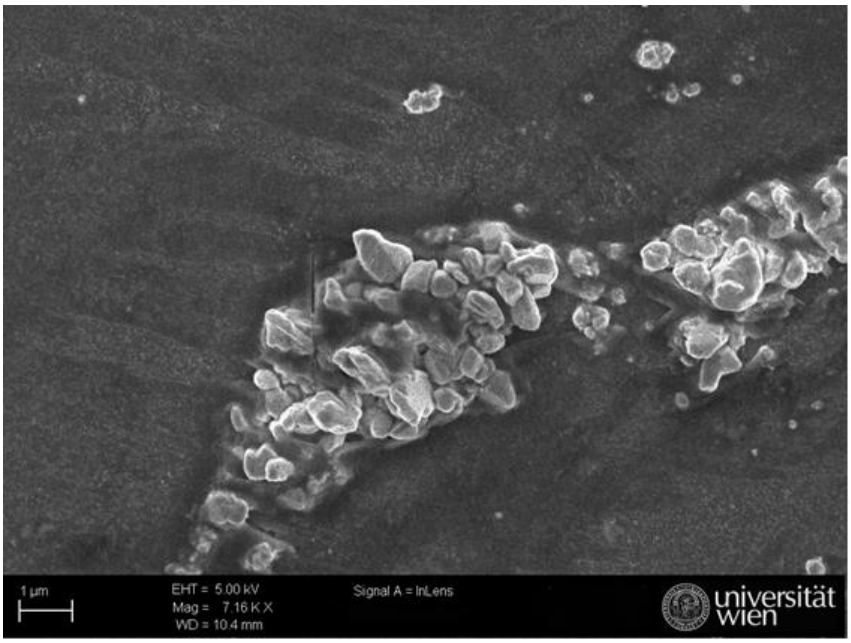

Figure 3.1. Scanning electron microscopy image of synthesized silver sulphide (Ag_2S) nanoparticle aggregates.

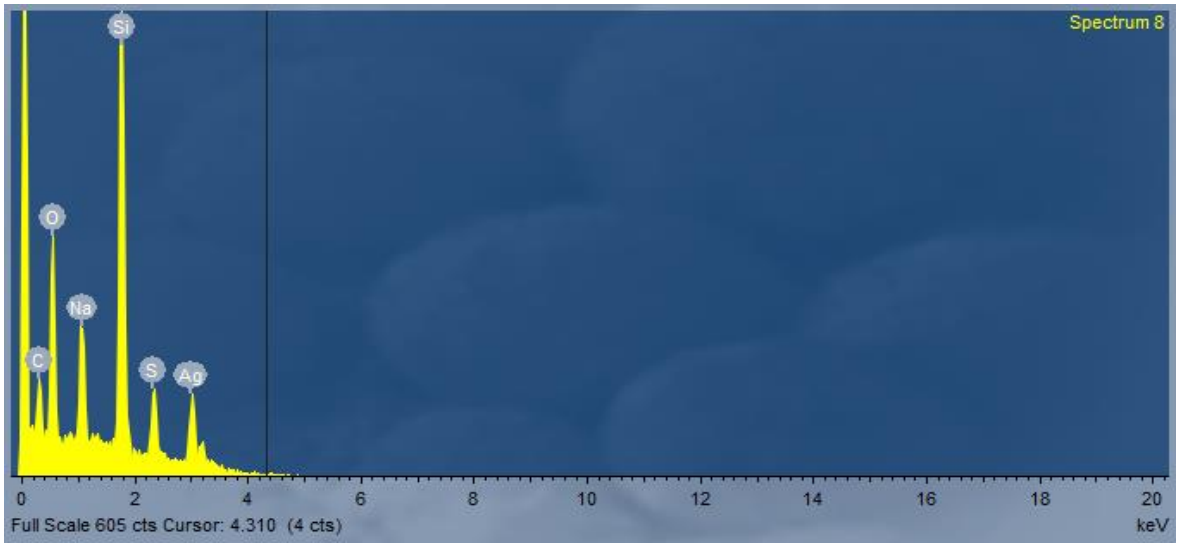

Figure 3.2. BSE spectrum of the SEM sample visualized in Figure 3.1.

Figure 3.2 demonstrates it is possible to ascertain peaks for silver and sulphur. As a result, this is an indication for the formation of Ag_2S NPs. The spectrum also shows the presence of silicon, from the substrate. Moreover, oxygen and sodium peaks can be seen. Presence of sodium and oxygen can be explained since they are originating from sodium thiosulfate during the synthesis process of the NPs. Finally, the carbon peak is attributed to the presence of PVP in the sample.

Focusing on single NPs allows for accurate evaluation of particle size. The small specimen depicted in Figure 3.3 measures circa 48 nm in cross-section. On the other hand, the NP in Figure 3.4 is characterized by a diameter of around 79 nm. It is thus hard to ensure that all particles have the same size. A possible solution is a more controlled environment for the synthesis of these NPs and a standardized speed of mixing the two agents ($AgNO_3$ and $Na_2S_20_3$) together. Images displaying the NPs lack some sharpness due to the hindrance evoked by the PVP molecules. As already explained, these water-soluble polymers allow for the stabilization of the NPs. However, eventually it is possible that some remnants of PVP remain present in between the particles.

Figure 3.3. SEM picture of a single silver sulphide nanoparticle.

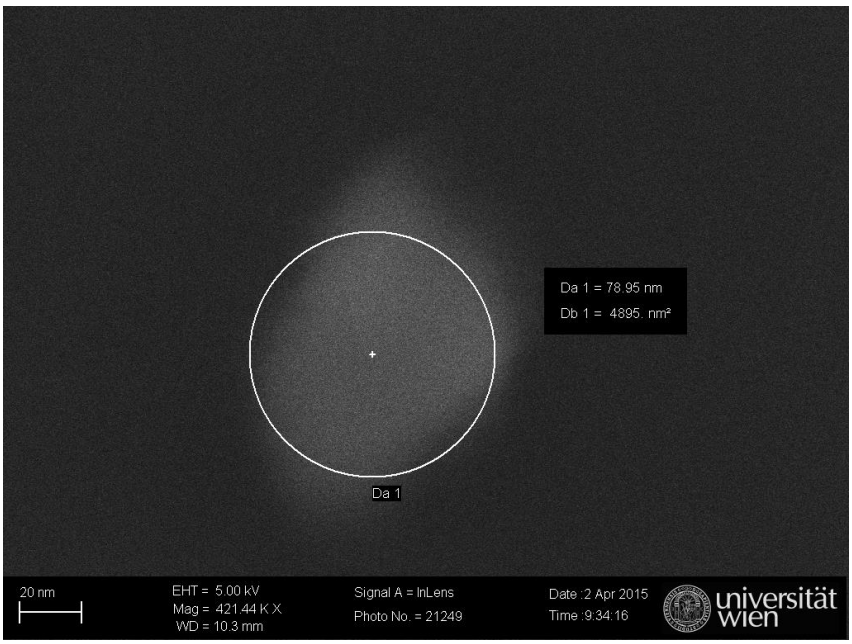

Figure 3.4. SEM picture of a single silver sulphide nanoparticle.

3.2. Quartz Crystal Microbalance

In a first attempt, the binding response of 1-butanol towards screen printed gold-coated quartz crystals microbalance is established. Out of this, it is possible to deduct the actual sensitivity of the VOC to NIPs, MIPs and composites. Concentrations BuOH are ranging from 1065 to 3368 ppm. The QCM response pattern obtained is given in Figure 3.5. The sensor characteristic, i.e. the frequency shifts as a function of butanol concentration are given in Table 3.1. For clarity, the first frequency shift corresponds to exposing the sensor to 1065 ppm 1-BuOH while the last one corresponds to 3368 ppm butanol.

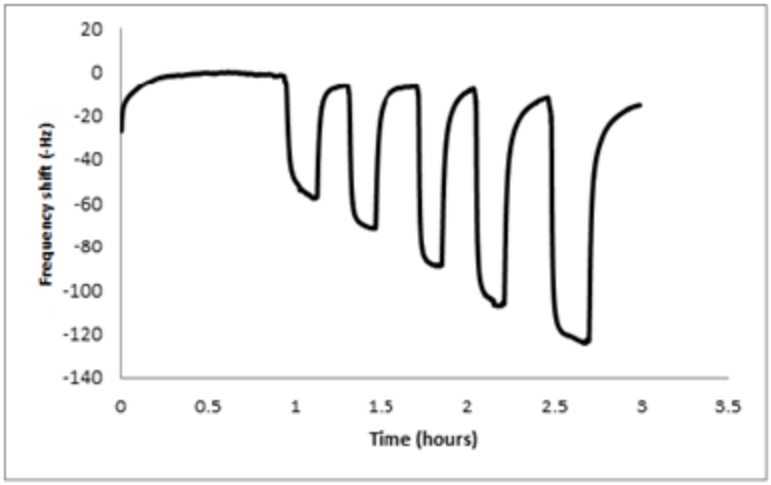

Figure 3.5. QCM response pattern of 1-butanol binding measured on non-functionalized gold electrode.

Table 3.1. Sensor characteristic resulting from data shown in Figure 3.5.

Concentration 1-butanol (ppm)	Frequency shift (Hz)
1065	- 55
1354	- 65
2019	- 81
2691	- 97
3368	- 110

Plotting these values results in a calibration curve represented in Figure 3.6. It clearly reveals linear response behaviour of the QCM to 1-butanol in the given concentration range. Below these values, one cannot observe sensor responses, as can be seen in Figure 3.7. At concentrations below 700 ppm, the sensor reveals no statically significant responses. Too high concentrations, on the other hand, lead to saturation of the gold electrode and thus of the related frequency signal. Moreover, investigating larger concentrations of 1-butanol is not of particular interest since that high amounts are not relevant to real-life measurements.

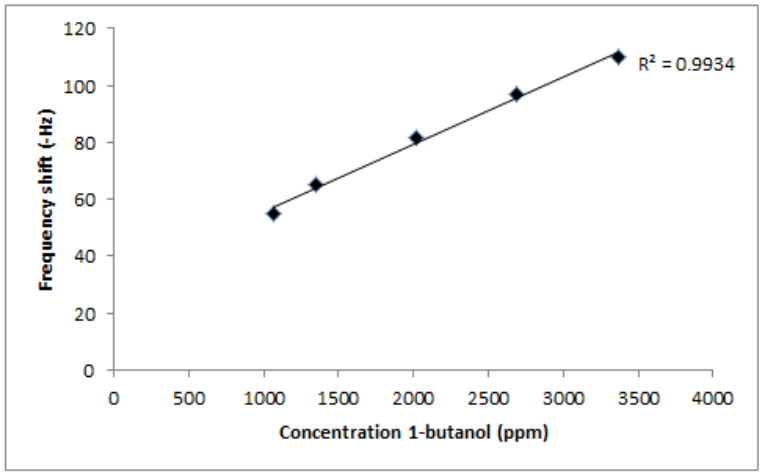

Figure 3.6. Sensor characteristics of a bare QCM towards 1-butanol. Only the linear range is visualized here.

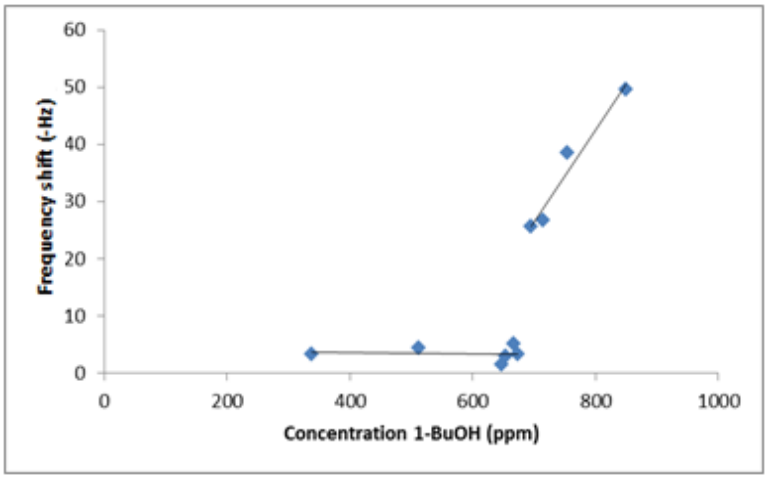

Figure 3.7. Full sensor characteristics of 1-butanol binding on a bare QCM sample showing the limit of detection (LOD).

After performing these standardization measurements, the response pattern of non-imprinted polymers towards 1-butanol is obtained. In contrast to MIP, this matrix lacks the tailor-made binding sites. Therefore, only unselective binding of 1-BuOH onto the surface is expected to occur. Doing so with an increasing amount of the VOC leads to the pattern displayed in Figure 3.9. It should be noted that after application of 3368 ppm 1-BuOH, an electronic error occurred making it impossible to further monitor the binding event. All butanol concentrations added here are located within the linear range of butanol saturation on bare gold QCM crystals (Figure 3.6).Most significant, the sensitivity of the polymer is substantially higher, than for the uncoated QCM. Furthermore, at this point, saturation is not yet taking place.

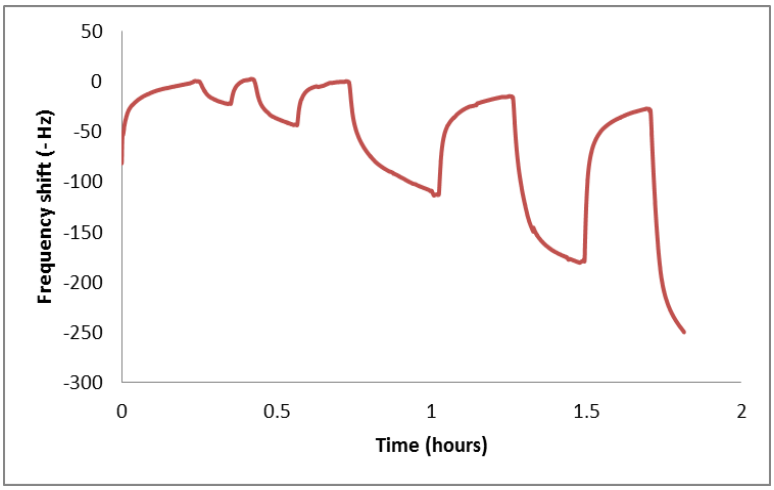

Figure 3.9. Frequency shifts after subjecting a MIP-coated QCM sample (A) to 1) 1065 ppm, 2) 1354 ppm, 3) 2019 ppm, 4) 2691 ppm and 5) 3368 ppm of 1-BuOH.

Unfortunately, attempts to determine the frequency differences after exposing NP-coated samples to various butanol concentrations have not been successful. This is because the nanoparticles are not covalently bound to the surface and the air/butanol stream will be strong enough to move them. This motion will result in a high noise ratio and makes it impossible to detect responses. A possible solution would be the immobilization of the Ag_2S NPs. Solely, it should be stated that one has to take in to account the effect of this linker molecule on selectivity/sensitivity towards 1-butanol.

Thereafter, similar measurements are performed using a QCM sample coated with polyurethane MIPs. In contrast to the NIPs, molecularly imprinted polymers are expected to contain specific binding sites to bind the gas molecules. Exposure to the same amounts of 1-butanol leads to the responses visualized in Figure 9.9A.

Furthermore, the same procedure is repeated for a composite coated with both NPs and PU MIPs. Because the NPs are embedded in the polymer matrix, it is feasible to execute QCM experiments while employing the gas streams. The final result is indicated in Figure 3.9B.

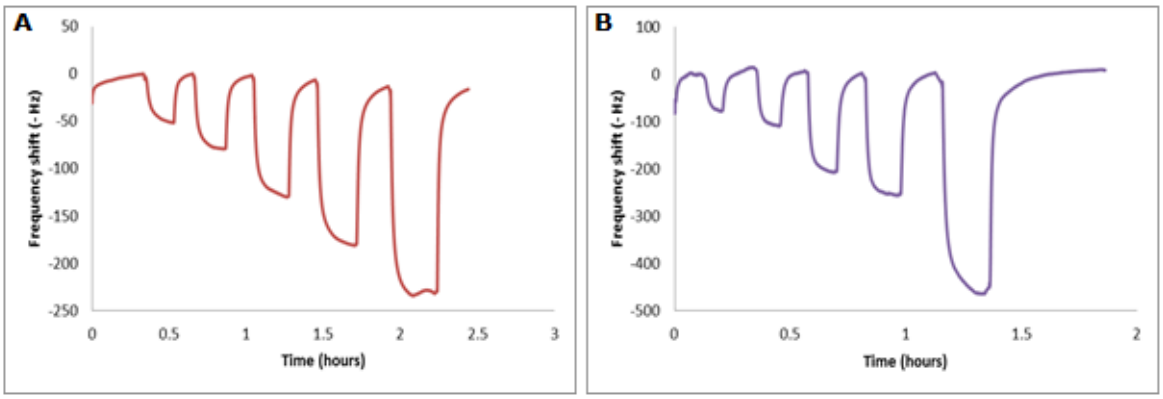

Figure 3.9. Frequency shifts after exposing a MIP-coated QCM sample (A) to 1) 1065 ppm, 2) 1354 ppm, 3) 2019 ppm, 4) 2691 ppm and 5) 3368 ppm of 1-BuOH. In (B), a composite is exposed to the same concentrations of BuOH.

Figure 3.10 summarizes the sensor responses towards 1-BuOH for uncoated, NIP-, MIP- and composite-coated samples. All frequency shifts are obtained by subtracting the first measured frequency value (0~10 MHz) from all later points. Composites significantly show the highest sensitivity towards 1-butanol. Exposition to 3368 ppm of BuOH results in a shift of ~ -470 Hz, which is more than twice the respective signal for MIP-coated quartzes. Furthermore, at larger concentration, it is possible to distinguish MIP- or NIP-coated samples and blank samples. At lower concentrations (less than 2000 ppm), this is not possible anymore. However, no clear distinction is observed between MIP and NIP sensitivity towards 1-BuOH.

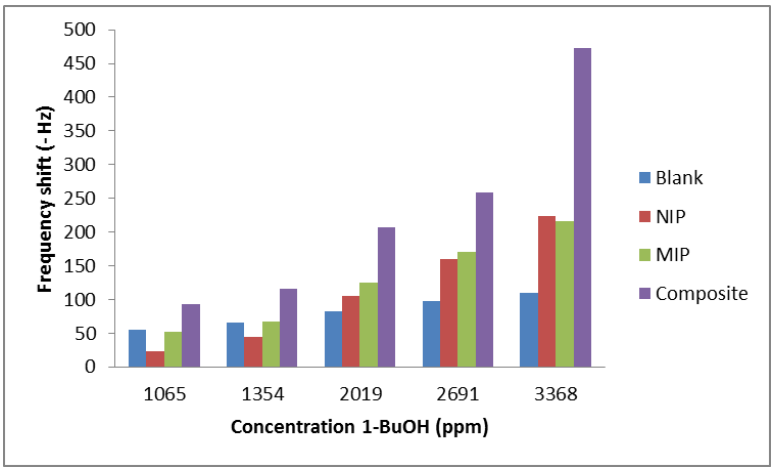

Figure 3.10. Sensor signals against 1-butanol. Frequency shifts are relative and not corrected for layer height.

Table 3.2. Concentrations 1-butanol and there related frequency shifts on blank, NIP-, MIP- and composite-coated substrates.

Concentration 1-BuOH (ppm)	Δf Blank (Hz)	Δf NIP (Hz)	Δf MIP (Hz)	Δf Composite (Hz)
1065	-55	-23	-52	-93
1354	-65	-44	-67	-116
2019	-82	-105	-125	-208
2691	-97	-159	-171	-259
3368	-110	-223	-218	-473

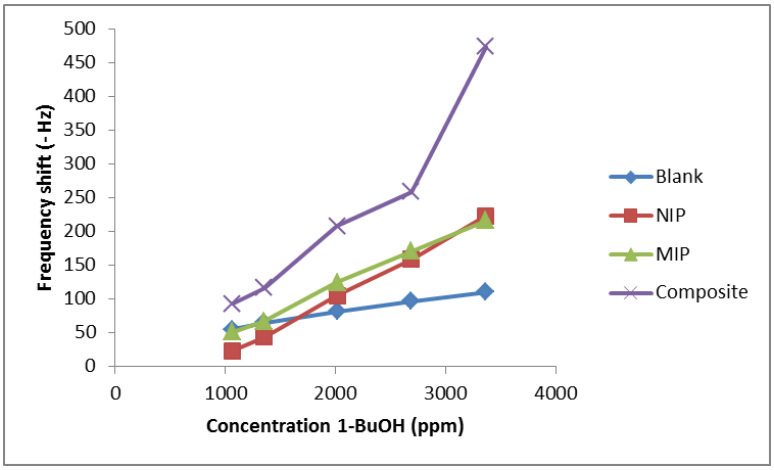

Figure 3.11. Sensor signals against 1-butanol. Frequency shifts are relative and not corrected for layer height.

It should however be noted that these layers have different heights. Performing frequency measurements on a network analyzer before and after coating resulted in changes of -19 kHz, -6.88 kHz and -5.31 kHz for NIP, MIP and composite, respectively. In terms of layer heights, this approximates to 760 nm for the NIP coated sample, 275 nm for the MIP and roughly 210 nm for the composite. This calculation is based on the assumption that 1 kHz frequency shift on a 10 MHz QCM corresponds to 40 nm layer height, which can be deduced from the Sauerbrey equation.

Hence, Figure 3.11 summarizes the QCM responses normalized to layer heights of NIP, MIP and composites, respectively. Relative frequency signals are displayed per kHz of coating. Compared to Figure 3.9, a more clear distinction between MIP and NIP is evident. As can be deducted from Table 3.3, composites show the highest QCM signal and thus affinity towards 1-butanol. The frequency shift of composites after application of 3368 ppm butanol is about three times higher than that of MIP. Moreover, composites are featured by an eight times higher response compared to NIP. Figure 3.13 gives a more clear indication about the differences in response towards 1-BuOH.

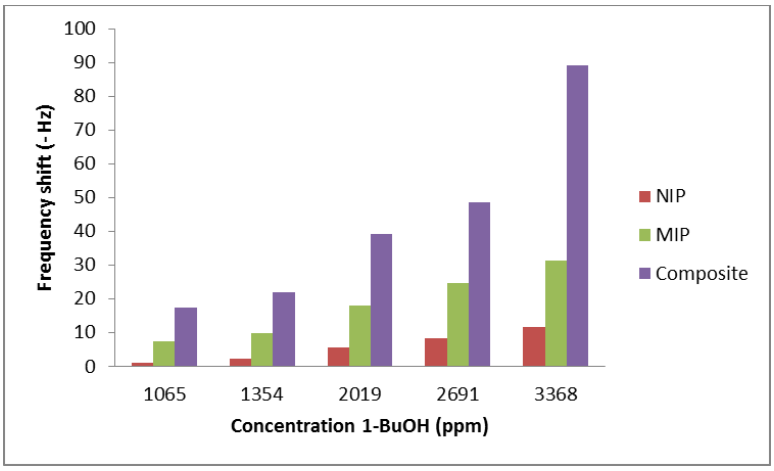

Figure 3.12. Sensor signals against 1-butanol corrected for layer height. Layer thicknesses are 760 nm, 275 nm and 212 nm for NIP, MIP and composite respectively.

Table 3.3. Concentrations 1-butanol and there related frequency shifts on blank, NIP-, MIP- and composite-coated substrates after correlation to layer heights.

Concentration 1-BuOH (ppm)	Δf NIP (Hz)	Δf MIP (Hz)	Δf Composite (Hz)
1065	-1	-7	-18
1354	-2	-9	-22
2019	-6	-18	-39
2691	-8	-25	-49
3368	-11	-32	-89

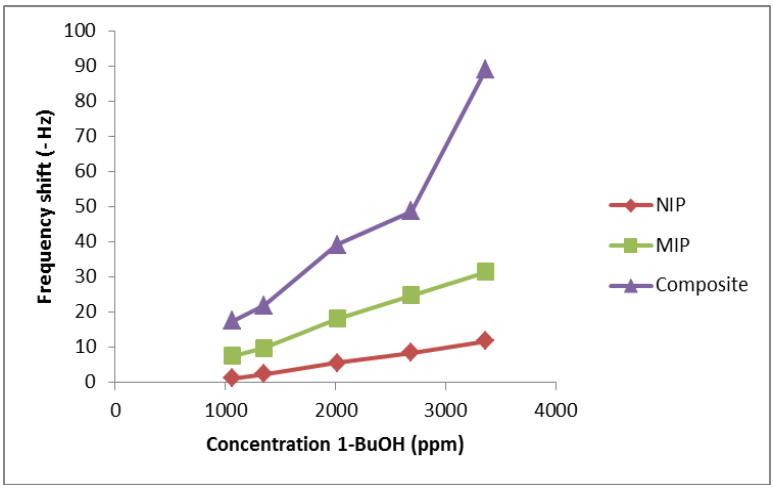

Figure 3.13. Sensor characteristics against 1-butanol. Frequency shifts are relative and corrected for layer height.

To conclude, the difference in response between MIPs and composites is evaluated. Composites clearly have a larger sensitivity towards the 1-BuOH. On average, composites are characterized by a signal which is twice as high as the one for MIPs exposed to equal concentrations of butanol. After correcting for layer thickness, it appears that the response of composites is even more significantly higher. Application of 3368 ppm of 1-BuOH leads to a ratio which amounts 2.19 before and 2.75 after correction. When exposing the QCM to lower concentrations, the same trend is observed, namely an increase in frequency shift after layer thickness correction. It cannot be stated that the ratio of frequency shift for composite to MIP will become larger with increasing concentrations of 1-BuOH.

Table 3.2. Ratio of Composite over MIP in function of frequency differences after exposition to various concentrations of 1-BuOH.

Concentration 1-BuOH (ppm)	Ratio Composite/MIP before Layer Thickness Correction	Ratio Composite/MIP after Layer Thickness Correction
1065	1.8	2.27
1354	1.73	2.18
2019	1.66	2.09
2691	1.51	1.9
3368	2.19	2.75

4. Conclusion & Future Outlook

To summarize, it can be stated that we have developed a novel method for the synthesis of silver sulphide (Ag_2S) nanoparticles. Beneficial for this method is that it bypasses the workplace safety issues related to H_2S, which normally are accompanied with the formation of these specific NPs. In contrast to for example the H_2S method, it is more convenient to handle and control the reaction conditions. These self-made NPs can then be incorporated in polyurethane (PU) matrices. Both components separately are able to specifically detect molecules and can be employed as sensor layers. NPs are able to capture VOCs because of chemically attractive interactions which are not yet fully understood. Preliminary studies already demonstrated that Ag_2S NPs show the largest sensitivity towards 1-BuOH. PU, on the other hand can be used in order to develop molecularly imprinted polymers having large affinity for 1-BuOH. The structure consisting of the NPs and PU is defined as a composite, a material having new properties distinct from the separate parts. It has been proven that together, they show even higher sensitivity towards small volatile organic compounds such as 1-butanol. It can be stated that composites show more than two times higher sensitivity towards 1-BuOH. According to our hypothesis, synergetic effects are responsible for this and the working mechanism has yet to be revealed. Furthermore, the response pattern of these composites is assessed after exposure to different concentrations of VOCs. A clear trend is observed indicating NIP, MIP and composites all show larger responses when exposed to higher concentrations of 1-BuOH. At these larger concentrations, the distinction between composites and MIPs become more manifest. Another objective, namely selectivity, has yet to be assessed based on experiments towards molecules with same chain length, but different functionality (i.e. butanethiol), or same functionality, but different steric properties. In the end, composites can be generated whose morphology is defined in a more unambiguously way.

In the past, precise determination of VOC concentrations was counteracted because of their narrow density in nature. Though, combining both sensitivity of Ag_2S NPs and selectivity of polyurethane MIPs results in a platform sensitive enough to assign correct concentrations. Gain insight in the working mechanism of this synergetic process allows one to further optimize the sensor responses in order to establish even more accurate measurements of these chemical compounds.

5. References

1. Barmark M. Social determinants of the sick building syndrome: exploring the interrelated effects of social position and psychosocial situation. Int J Environ Health Res. 2014:1-18.
2. Norhidayah A, Chi-Kuang L, Azhar MK, Nurulwahida S. Indoor Air Quality and Sick Building Syndrome in Three Selected Buildings. 2013. p. 93-8.
3. Maoz-Segal R, Agmon-Levin N, Israeli E, Shoenfeld Y. [The sick building syndrome as a part of 'ASIA' (autoimmune/auto-inflammatory syndrome induced by adjuvants)]. Harefuah. 2015;154(2):129-32, 34.
4. Zhang X, Li F, Zhang L, Zhao Z, Norback D. A longitudinal study of sick building syndrome (SBS) among pupils in relation to SO2, NO2, O3 and PM10 in schools in China. PLoS One. 2014;9(11):e112933.
5. Joann Ten B, Steve S, Alfred TH, William JF, Mark JM, Catherine PK, et al. Development of New Volatile Organic Compound (VOC) Exposure Metrics and their Relationship to "Sick Building Syndrome" SymptomsDevelopment of new VOC exposure metrics and their relationship to sick building syndrome symptoms. Indoor Air. 1998;8(3).
6. Joshi SM. The sick building syndrome. Indian Journal of Occupational and Environmental Medicine. 2008;12(2):61-4.
7. Petersen S, Jensen KL, Pedersen AL, Rasmussen HS. The effect of increased classroom ventilation rate indicated by reduced CO concentration on the performance of schoolwork by children. Indoor Air. 2015.
8. Abdel-Hamid MA, S AH, Elokda EE, Mostafa NS. Prevalence and risk factors of sick building syndrome among office workers. J Egypt Public Health Assoc. 88. England2013. p. 109-14.
9. Mishra N, Bartsch J, Ayoko GA, Salthammer T, Morawska L. Volatile Organic Compounds: Characteristics, distribution and sources in urban schools. Atmospheric Environment. 2015;106(0):485-91.
10. Atkinson R, Arey J. Atmospheric degradation of volatile organic compounds. Chem Rev. 2003;103(12):4605-38.
11. Tanaka-Kagawa T, Furuta M, Shibatsuji M, Jinno H, Nishimura T. [Volatile organic compounds (VOCs) emitted from large furniture]. Kokuritsu Iyakuhin Shokuhin Eisei Kenkyusho Hokoku. 2011(129):76-85.
12. Ho DX, Kim KH, Sohn JR, Oh YH, Ahn JW. Emission rates of volatile organic compounds released from newly produced household furniture products using a large-scale chamber testing method. ScientificWorldJournal. 2011;11:1597-622.
13. Xue L, Wang T, Wang X, Blake DR, Gao J, Nie W, et al. On the use of an explicit chemical mechanism to dissect peroxy acetyl nitrate formation. Environ Pollut. 2014;195:39-47.
14. Taylor OC. Importance of peroxyacetyl nitrate (PAN) as a phytotoxic air pollutant. J Air Pollut Control Assoc. 1969;19(5):347-51.
15. Heddle JA, Shepson PB, Gingerich JD, So KW. Mutagenicity of peroxyacetyl nitrate (PAN) in vivo: tests for somatic mutations and chromosomal aberrations. Environ Mol Mutagen. 1993;21(1):58-66.
16. Russell JA, Hu Y, Chau L, Pauliushchyk M, Anastopoulos I, Anandan S, et al. Indoor-Biofilter Growth and Exposure to Airborne Chemicals Drive Similar Changes in Plant Root Bacterial Communities. Applied and Environmental Microbiology. 2014;80(16):4805-13.
17. Carrer P, Maroni M, Alcini D, Cavallo D. Allergens in indoor air: environmental assessment and health effects. Sci Total Environ. 2001;270(1-3):33-42.
18. Su F-C, Mukherjee B, Batterman S. Determinants of personal, indoor and outdoor VOC concentrations: An analysis of the RIOPA data. Environmental research. 2013;126:192-203.
19. Sekhar PK, Brosha EL, Mukundan R, Garzon FH. Chemical Sensors for Environmental Monitoring and Homeland Security. The Electrochemical Society Interface2010.
20. Vashist SK, Vashist P. Recent Advances in Quartz Crystal Microbalance-Based Sensors. 2011. p. 1-13.
21. Fan X, Du B. Selective detection of trace 1-butanol by QCM sensor coated with copolymer P(HEMA-*co*-MA). Sensors and Actuators B: Chemical. 2011;160:724-9.
22. Vasapollo G, Sole RD, Mergola L, Lazzoi MR, Scardino A, Scorrano S, et al. Molecularly Imprinted Polymers: Present and Future Prospective. International Journal of Molecular Sciences. 2011;12(9):5908-45.

23. Wackers G, Vandenryt T, Cornelis P, Kellens E, Thoelen R, De Ceuninck W, et al. Array Formatting of the Heat-Transfer Method (HTM) for the Detection of Small Organic Molecules by Molecularly Imprinted Polymers. Sensors (Basel, Switzerland). 2014;14(6):11016-30.
24. Chen L, Xu S, Li J. Recent advances in molecular imprinting technology: current status, challenges and highlighted applications. Chemical Society Reviews. 2011;40(5):2922-42.
25. Gal J, Cintas P. Early history of the recognition of molecular biochirality. Top Curr Chem. 2013;333:1-40.
26. Schirhagl R. Bioapplications for molecularly imprinted polymers. Anal Chem. 2014;86(1):250-61.
27. Zhang H. Water-compatible molecularly imprinted polymers: Promising synthetic substitutes for biological receptors. Polymer. 2014;55(3):699-714.
28. Algieri C, Drioli E, Guzzo L, Donato L. Bio-mimetic sensors based on molecularly imprinted membranes. Sensors (Basel). 14. Switzerland2014. p. 13863-912.
29. Perez-Moral N, Mayes AG. Direct rapid synthesis of MIP beads in SPE cartridges. Biosens Bioelectron. 21. England2006. p. 1798-803.
30. van Nostrum CF. Molecular imprinting: A new tool for drug innovation. Drug Discov Today Technol. 2005;2(1):119-24.
31. Alenus J, Ethirajan A, Horemans F, Weustenraed A, Csipai P, Gruber J, et al. Molecularly imprinted polymers as synthetic receptors for the QCM-D-based detection of L-nicotine in diluted saliva and urine samples. Anal Bioanal Chem. 2013;405(20):6479-87.
32. Peeters M, Csipai P, Geerets B, Weustenraed A, van Grinsven B, Thoelen R, et al. Heat-transfer-based detection of L-nicotine, histamine, and serotonin using molecularly imprinted polymers as biomimetic receptors. Anal Bioanal Chem. 2013;405(20):6453-60.
33. Mustafa G, Lieberzeit P. Molecularly imprinted polymer-Ag2S nanoparticle composites for sensing volatile organics. RSC Advances. 2014;4(25):12723-8.
34. Mustafa G. Soft Metal Sulfide Nanoparticles and Nanocomposite Based Sensors for Thiol and Alcohol Detection University of Vienna; 2011.
35. Krylova V, Dukštienė N. Synthesis and Characterization of Ag2S Layers Formed on Polypropylene. Journal of Chemistry2013. p. 1-11.
36. Wang D, Dimonie VL, Sudol ED, El-Aasser MS. Effect of PVP in Dispersion and Seeded Dispersion Polymerizations. 2002. p. 2721-32.
37. Sarkar A, Daniels-Race T. Electrophoretic Deposition of Carbon Nanotubes on 3-Amino-Propyl-Triethoxysilane (APTES) Surface Functionalized Silicon Substrates. 2013. p. 272-88.

6. Abbreviations

1-BuOH	1-butanol
AFM	Atomic force microscopy
Ag_2S	Silver sulfide
APTES	(3-Aminopropyl) triethoxysilane
BPA	Bisphenol A
CNS	Central nervous system
Cu_2S	Copper sulfide
DABCO	1,4-diazabicyclo[2.2.2]octane
dH_20	Distilled water
FTIR	Fourier transform infrared
H_2O_2	Hydrogen peroxide
H_2S	Hydrogen sulfide
H_2SO_4	sulfuric acid
MDI	4,4'-methylenediphenyl diisocyanate
MIP	Molecularly imprinted polymer
MoS_2	Molybdenum disulfide
MS	Mass spectrometry
$Na_2S_2O_3$	Sodium thiosulfate
NaOH	Sodium hydroxide
NO	Nitrogen oxide
NO_2	Nitrogen dioxide
NP	Nanoparticle
PAN	Peroxyacetyl nitrates
PU	Polyurethane
QCM	Quartz crystal microbalance
RPM	Revolutions per minute
SBS	Sick building syndrome
SEM	Scanning electron microscopy
THF	Tetrahydrofuran
UV-VIS	Ultraviolet-visible
VOC	Volatile organic compound

Auteursrechtelijke overeenkomst

Ik/wij verlenen het wereldwijde auteursrecht voor de ingediende eindverhandeling:
Defining the synergetic pattern of composites for sensing volatile organic compounds

Richting: **master in de biomedische wetenschappen-bio-elektronica en nanotechnologie**
Jaar: **2015**

in alle mogelijke mediaformaten, - bestaande en in de toekomst te ontwikkelen - , aan de Universiteit Hasselt.

Niet tegenstaand deze toekenning van het auteursrecht aan de Universiteit Hasselt behoud ik als auteur het recht om de eindverhandeling, - in zijn geheel of gedeeltelijk -, vrij te reproduceren, (her)publiceren of distribueren zonder de toelating te moeten verkrijgen van de Universiteit Hasselt.

Ik bevestig dat de eindverhandeling mijn origineel werk is, en dat ik het recht heb om de rechten te verlenen die in deze overeenkomst worden beschreven. Ik verklaar tevens dat de eindverhandeling, naar mijn weten, het auteursrecht van anderen niet overtreedt.

Ik verklaar tevens dat ik voor het materiaal in de eindverhandeling dat beschermd wordt door het auteursrecht, de nodige toelatingen heb verkregen zodat ik deze ook aan de Universiteit Hasselt kan overdragen en dat dit duidelijk in de tekst en inhoud van de eindverhandeling werd genotificeerd.

Universiteit Hasselt zal mij als auteur(s) van de eindverhandeling identificeren en zal geen wijzigingen aanbrengen aan de eindverhandeling, uitgezonderd deze toegelaten door deze overeenkomst.

Voor akkoord,

Cuypers, Wim

Datum: **9/06/2015**